Structural understanding of a polymorphic system by structure solution and refinement from powder X-ray diffraction data: the α and β phases of the latent pigment DPP-Boc †

Elizabeth J. MacLean,[a]‡ Maryjane Tremayne,[b] Benson M. Kariuki,[b] Kenneth D. M. Harris,*[b] Abul F. M. Iqbal[c] and Zhimin Hao[c]

[a] *Department of Chemistry, University College London, 20 Gordon Street, London, UK WC1H 0AJ*
[b] *School of Chemistry, University of Birmingham, Edgbaston, Birmingham, UK B15 2TT*
[c] *Ciba Specialty Chemicals Inc., Pigments Division, Postfach, R-1047.1.20, CH-4002 Basel, Switzerland*

Received (in Cambridge, UK) 9th February 2000, Accepted 14th April 2000
Published on the Web 26th May 2000

The latent pigment 1,4-dioxo-2,5-di-*tert*-butoxycarbonyl-3,6-diphenyl-1,2,4,5-tetrahydropyrrolo[3,4-*c*]pyrrole (abbreviated DPP-Boc) has been found to exist in the solid state in two polymorphic forms, denoted the α and β phases. Above ambient temperature, a thermal decomposition reaction occurs in both polymorphs to produce the commercially important pigment DPP. Significant differences have been observed in kinetic aspects of this reaction in the α and β phases, and such differences in reactivity must ultimately originate from structural differences between the two polymorphs. In this paper we focus on establishing a structural understanding of these materials. The structure of the α phase of DPP-Boc has been determined previously from single crystal X-ray diffraction data, although certain features of the reported structure are unsatisfactory. Here we report a revised structure determination of the α phase by Rietveld refinement from powder X-ray diffraction data. The structure of the β phase of DPP-Boc, which was previously unknown, has been solved directly from powder X-ray diffraction data using our Monte Carlo technique and Rietveld refinement. A detailed description and comparison of the structural properties of the α and β phases of DPP-Boc is presented.

1. Introduction

The phenomenon of polymorphism[1–3] has many important consequences with regard to the properties and applications of molecular materials. A polymorphic system comprises a set of crystalline materials with the same chemical composition, but with different crystal structures. For molecular solids, polymorphism arises when a given type of molecule forms different crystal structures—in many cases the molecule may adopt a different conformation in the different polymorphs (so-called conformational polymorphism). As all properties of solids depend directly on the structural characteristics of the solid, it is clear that the properties of polymorphs may differ significantly (even though they contain the same molecule). Thus, in both fundamental and applied contexts, it is important to understand the structural characteristics of different polymorphs. In the field of high-performance pigments there are many examples of polymorphism (*e.g.* quinacridones,[4] DTPP,[5,6] diethyl 2,5-diaminoterephthalate[7]); importantly, the different polymorphic forms of these pigment materials can differ significantly in terms of their colouristic properties.

Although single crystal X-ray diffraction is the most powerful tool for elucidating crystal and molecular structures, the requirement for single crystal samples of sufficient size and quality limits the scope of this technique, as many materials of interest cannot be prepared in this form. Progress in the structural characterization of such materials relies heavily on the availability of techniques to allow crystal structures to be determined directly from powder diffraction data. Here we report structural characterization of such an example, based on polymorphs of the pigment precursor ("latent" pigment) 1,4-dioxo-2,5-di-*tert*-butoxycarbonyl-3,6-diphenyl-1,2,4,5-tetrahydropyrrolo[3,4-*c*]pyrrole (DPP-Boc) (Scheme 1).

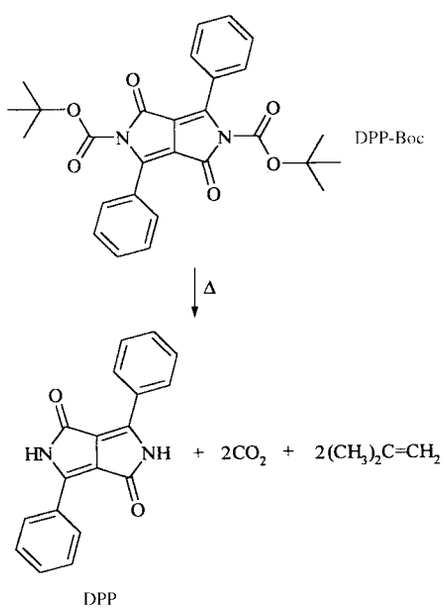

Scheme 1 Molecular structure of the latent pigment DPP-Boc, and the thermal reaction to produce the commercial pigment DPP.

† Colour plots showing crystal structures of α-DPP-Boc viewed along the *a*- and *c*-axes and of β-DPP-Boc viewed along the *a*-axis are available as supplementary data. For direct electronic access see http://www.rsc.org/suppdata/p2/b0/b001108h/

‡ Present address: Daresbury Laboratory, Daresbury, Warrington, UK WA4 4AD.

DOI: 10.1039/b001108h

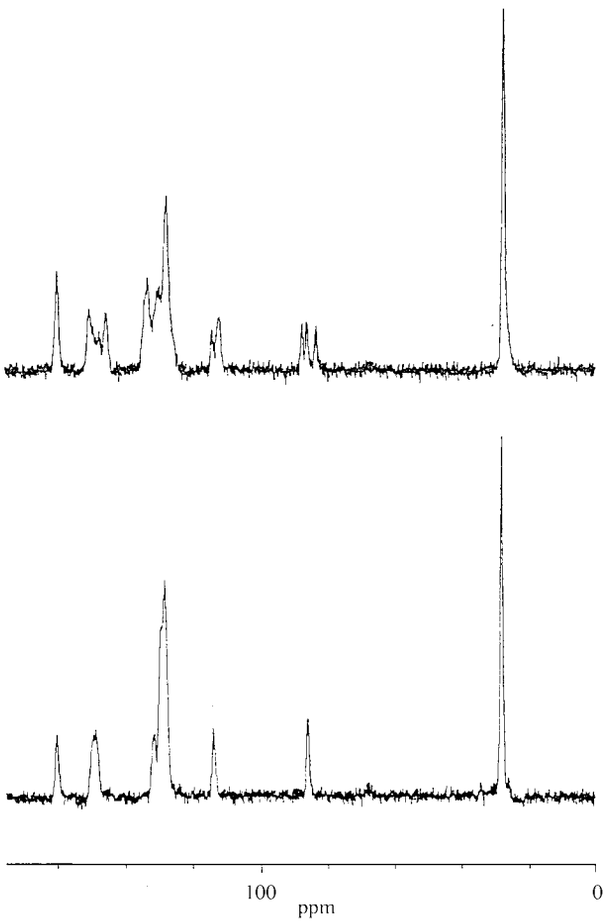

Fig. 1 High-resolution solid state ^{13}C NMR spectra of α-DPP-Boc (top) and β-DPP-Boc (bottom).

By definition, pigments are coloured solid particles that are insoluble in the medium in which the pigment is applied (for example, in paints, plastics and printing inks). Due to the insolubility of pigments, obtaining a homogeneous colouration requires the ability to control the dispersion of the pigment particles in the application medium. An approach developed recently[8,9] to ensure good dispersion is to introduce the pigment chromophore as a molecule (pigment precursor or "latent" pigment) which is readily soluble in the application medium. Subsequently, the insoluble pigment particles are generated *in situ* through an appropriate chemical reaction of the latent pigment. An illustration is the latent pigment DPP-Boc, which undergoes a thermal reaction (involving removal of the *tert*-butoxycarbonyl group) to produce the commercial red pigment DPP (Scheme 1). In addition to the exploitation of this reaction in a variety of different applications media, this reaction is also known to take place in the crystalline phases of DPP-Boc, resulting in a solid–solid transformation[10] to produce (ultimately) DPP.[8,9]

The latent pigment DPP-Boc has been found to exist in two polymorphic forms, which we denote as the α and β phases. We have shown[10] that the reaction to produce the pigment DPP occurs (at high temperature) in both solid phases, but with significant differences in kinetic aspects of the reaction in each polymorph. Ultimately, such differences in reactivity must originate from structural differences between the two polymorphs, and we focus in this paper on establishing a structural understanding of these materials.

The structure of the α phase of DPP-Boc has been determined previously from single crystal X-ray diffraction data.[11] Rather unusually, the asymmetric unit contains three independent half molecules, as confirmed by high-resolution solid state ^{13}C NMR (for several carbon environments within the molecule, three peaks of essentially equal intensity are observed in the ^{13}C NMR spectrum (Fig. 1)). During routine diffraction experiments, a second polymorph of DPP-Boc has been discovered. High-resolution solid state ^{13}C NMR has provided some insights[12] concerning structural properties of this polymorph. Thus, the ^{13}C NMR spectrum for β-DPP-Boc has only a single peak for each carbon environment in the molecule (Fig. 1), implying that the asymmetric unit comprises only one half molecule (*i.e.* with the molecular inversion centre located on a crystallographic inversion centre).

In order to determine the crystal structure of β-DPP-Boc, attempts were made to prepare crystals of sufficient size and quality for single crystal X-ray diffraction experiments, but these attempts were unsuccessful. Instead, the crystal structure of β-DPP-Boc has been solved from powder X-ray diffraction data using our Monte Carlo technique[13–15] and refined subsequently using Rietveld refinement.[16] The crystal structure of α-DPP-Boc has also been refined in this work from powder X-ray diffraction data using the Rietveld method, leading to an improved description of the structural properties of this polymorph.

2. Background to powder structure solution

Although traditional techniques[17–21] for structure solution from powder diffraction data have been applied successfully in several cases, these techniques have certain intrinsic limitations[17] and organic molecular crystals represent a particularly challenging case. For these reasons, there has been considerable interest in recent years in the development of new methods for solving crystal structures directly from powder diffraction data, leading *inter alia* to a new generation of "direct-space" approaches. In the direct-space strategy,[13,17,22] trial crystal structures are sampled in direct space, with the "quality" of each trial structure assessed by comparing the calculated powder diffraction pattern for the trial structure and the experimental powder diffraction pattern. In our work, this comparison is quantified on the basis of the profile *R*-factor R_{wp},[17] which considers the whole digitized intensity profile and implicitly takes care of peak overlap. The structure solution process effectively involves searching a hypersurface $R_{wp}(\Gamma)$ to find the best structure solution (lowest R_{wp}), where Γ represents the set of variables that define the trial structures. For the case of one molecule in the asymmetric unit, the variables in Γ represent the position $\{x, y, z\}$, orientation $\{\theta, \varphi, \psi\}$ and intramolecular geometry (specified by variable torsion angles $\{\tau_1, \tau_2, ..., \tau_n\}$) of the molecule. In general, the bond lengths and bond angles (and any known torsion angles) are fixed in the calculation, and are taken either from standard values for the type of molecule under investigation or from the known geometries of similar molecules. Methods used to search *R*-factor (or in some cases χ^2) hypersurfaces to locate the global minimum within direct-space structure solution strategies have included Monte Carlo,[13–15,17] simulated annealing[22–27] and Genetic Algorithm[28–32] techniques. Here we focus on the application of our Monte Carlo method.

3. Experimental

For α-DPP-Boc, a polycrystalline sample was ground and mounted in a rotating disc between two layers of transparent tape. The powder X-ray diffraction pattern of this sample was recorded in transmission mode on a Siemens D5000 diffractometer using $CuK_{\alpha 1}$ radiation (Ge-monochromated) and a conventional scintillation counter. The total data range was $4° \leq 2\theta \leq 50°$, measured in steps of 0.02° over a total data collection time of 38 hours.

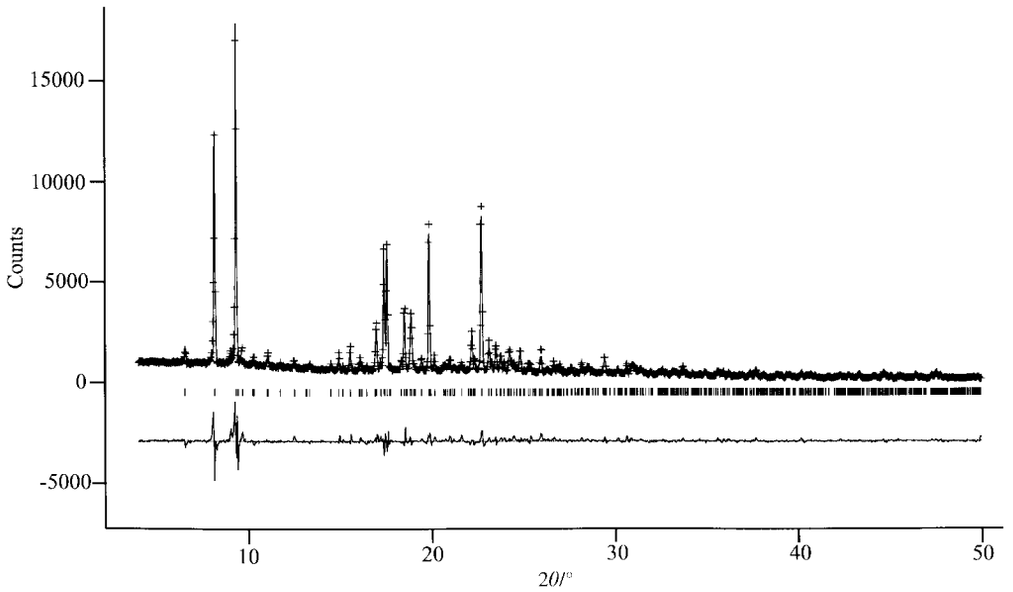

Fig. 2 Experimental (+), calculated (solid line) and difference (bottom) powder diffraction profiles for the final Rietveld refinement of α-DPP-Boc. Reflection positions are marked.

For β-DPP-Boc, a polycrystalline sample was ground and loaded into a capillary (1.0 mm diameter) and mounted on the high-resolution powder diffractometer on Station 2.3[33,34] at the Synchrotron Radiation Source, Daresbury Laboratory. The powder X-ray diffraction pattern was recorded at $\lambda = 1.4000$ Å. The total data range was $5° \leq 2\theta \leq 60°$, measured in steps of 0.01° over a total data collection time of 5 hours.

4. Preliminary analysis

The powder X-ray diffraction pattern of α-DPP-Boc was indexed using the program ITO[35] on the basis of the first 20 observable reflections, leading to the lattice parameters (monoclinic metric): $a = 10.50$ Å, $b = 21.49$ Å, $c = 17.16$ Å, $\beta = 95.3°$. Systematic absences are consistent with space group $P2_1/n$. These lattice parameters and space group are in agreement with those obtained previously[11] from single crystal X-ray diffraction data [$a = 10.497$ Å, $b = 21.517$ Å, $c = 17.176$ Å, $\beta = 95.14°$].

The powder X-ray diffraction pattern of β-DPP-Boc was also indexed using the program ITO[35] on the basis of the first 20 observable reflections, leading to the lattice parameters (monoclinic metric): $a = 6.23$ Å, $b = 10.30$ Å, $c = 19.47$ Å, $\beta = 90.4°$. Systematic absences are consistent with space group $P2_1/c$. The unit cell volume of β-DPP-Boc is 1250 Å^3, in comparison with 3866 Å^3 for α-DPP-Boc, consistent with the assignment of six molecules per unit cell for α-DPP-Boc and two molecules per unit cell for β-DPP-Boc.

5. Structure refinement of α-DPP-Boc

Our analysis of the powder X-ray diffraction data for α-DPP-Boc used the structure reported previously[11] as the starting point for Rietveld refinement using the GSAS program package.[36] The molecular geometry in the structure reported previously was rather distorted, particularly with regard to the phenyl rings. Hydrogen atoms were placed in calculated positions on the phenyl rings and the positions of all atoms were refined (note that the structure determined previously[11] from single crystal X-ray diffraction data did not contain hydrogen atoms). For all atoms of a given type, the isotropic displacement parameters were constrained to a common value and allowed to refine, except for the hydrogen atoms for which the common isotropic displacement parameter was fixed at 0.05 Å^2. Standard restraints were applied to bond lengths and bond angles. Final convergence was achieved (Fig. 2) with $R_{wp} = 11.6\%$, $R_p = 7.7\%$ and $\chi^2 = 9.4$ (2300 data points and 230 refined parameters). The final refined crystal structure is shown in Fig. 3, and atomic coordinates are reported in Table 1. There are three half molecules in the asymmetric unit. Two of the half molecules represent one complete molecule with no internal symmetry (which we refer to as the "asymmetric molecule"), and the other half molecule is located such that the midpoint of the central C–C bond of the pyrrolo[3,4-*c*]pyrrole unit is located on a crystallographic inversion centre, thus giving rise to a centrosymmetric molecule (which we refer to as the "symmetric molecule"). The unit cell thus contains four asymmetric molecules and two symmetric molecules. We note that the peaks at $2\theta \approx 8.2°$ and 9.4° in the experimental powder diffraction pattern have significant asymmetry, representing a substantial contribution to the discrepancy between the calculated and experimental powder diffraction data (Fig. 2).

From the powder diffraction pattern, it is clear that the sample of α-DPP-Boc used in this work contains trace amounts of β-DPP-Boc (peaks at $2\theta \approx 9.1°$ and 9.7°). We were unable to find a method to remove the β phase by selective dissolution, as both polymorphs have comparable solubilities in most common solvents. While we could, in principle, exclude regions containing impurity peaks from the refinement, the significant overlap of peaks from the two phases precludes this action. We note that, following the determination of the crystal structure of β-DPP-Boc (see Section 6), a simultaneous refinement of the two phases could be carried out using the powder diffraction data described above for α-DPP-Boc.

The crystal structure of α-DPP-Boc (Fig. 3) contains columns of DPP-Boc molecules stacked along the *c*-axis. The molecules in adjacent columns are packed relative to each other in a herring-bone manner, as shown in Fig. 3(b). Within the repeat distance along the column axis, there is one symmetric molecule and two asymmetric molecules, with the two asymmetric molecules related to each other across the inversion centre. The structure of α-DPP-Boc is discussed in more detail in Section 7.

6. Structure solution and refinement of β-DPP-Boc

The crystal structure of β-DPP-Boc was unknown prior to the present work, in which we have solved this structure directly from powder diffraction data using our Monte Carlo method. In the Monte Carlo calculations, the structural fragment (Fig. 4) comprised all atoms of the asymmetric unit (excluding

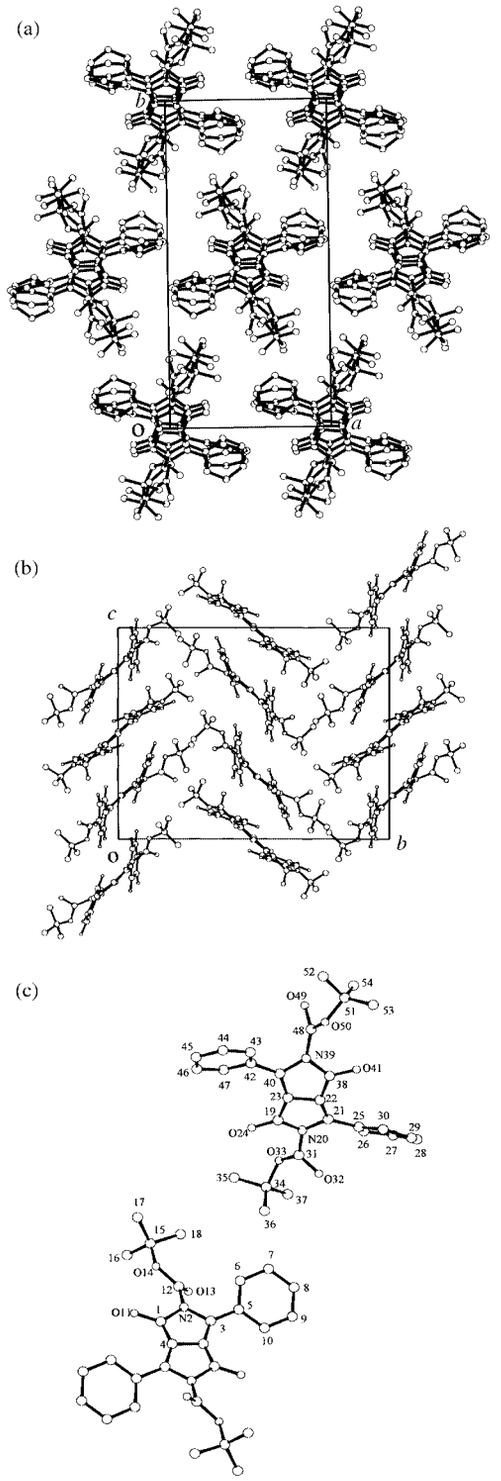

Fig. 3 Crystal structure of α-DPP-Boc viewed (a) along the column axis (*c*-axis) and (b) along the *a*-axis (almost perpendicular to the column axis). Note that the complete contents of the unit cell are shown (with three independent half molecules along the column axis in the asymmetric unit). The atom labelling scheme (with the label C for each carbon atom omitted for clarity) is defined in (c), for the three independent half molecules viewed along the column axis.

hydrogen atoms), comprising half the DPP-Boc molecule with the molecular inversion centre constrained to reside on the crystallographic inversion centre. In the Monte Carlo calculation, "global" rotation of the structural fragment was carried out by random angular displacements around a randomly chosen axis constrained to pass through the inversion centre (denoted × in Fig. 4), and the molecular geometry was varied by random displacements of four torsion angles (three torsion angles within the *tert*-butoxycarbonyl group and one torsion angle connecting the phenyl ring to the pyrrolo[3,4-*c*]pyrrole unit—see Fig. 4). Note that translation of the structural frag-

Table 1 Final refined atomic coordinates and isotropic displacement parameters for α-DPP-Boc [$P2_1/n$; $a = 10.4851(4)$ Å, $b = 21.4631(6)$ Å, $c = 17.1342(1)$ Å, $\beta = 95.245(2)°$]. Atom labelling is defined in Fig. 3(c)

Atom	*x*	*y*	*z*	U_{iso}/Å²
C1	−0.614(1)	−0.453(1)	−0.053(1)	0.009(2)
N2	−0.515(1)	−0.423(1)	−0.089(1)	0.061(4)
C3	−0.403(1)	−0.452(1)	−0.057(1)	0.009(2)
C4	−0.434(1)	−0.500(1)	−0.005(1)	0.009(2)
C5	−0.282(1)	−0.428(1)	−0.082(1)	0.009(2)
C6	−0.275(1)	−0.368(1)	−0.111(1)	0.009(2)
C7	−0.156(1)	−0.343(1)	−0.127(1)	0.009(2)
C8	−0.049(1)	−0.382(1)	−0.125(1)	0.009(2)
C9	−0.056(1)	−0.443(1)	−0.095(1)	0.009(2)
C10	−0.174(1)	−0.467(1)	−0.078(1)	0.009(2)
O11	−0.727(1)	−0.435(1)	−0.059(1)	0.083(5)
C12	−0.537(1)	−0.379(1)	−0.149(1)	0.009(2)
O13	−0.496(1)	−0.390(1)	−0.213(1)	0.083(5)
O14	−0.633(1)	−0.337(1)	−0.150(1)	0.083(5)
C15	−0.657(1)	−0.289(1)	−0.205(1)	0.009(2)
C16	−0.756(1)	−0.313(1)	−0.270(1)	0.009(2)
C17	−0.711(1)	−0.234(1)	−0.161(1)	0.009(2)
C18	−0.529(1)	−0.270(1)	−0.236(1)	0.009(2)
C19	−0.114(1)	−0.031(1)	0.149(1)	0.009(2)
N20	−0.011(1)	−0.052(1)	0.108(1)	0.061(4)
C21	0.099(1)	−0.029(1)	0.147(1)	0.009(2)
C22	0.064(1)	0.011(1)	0.205(1)	0.009(2)
C23	−0.072(1)	0.016(1)	0.206(1)	0.009(2)
O24	−0.225(1)	−0.047(1)	0.131(1)	0.083(5)
C25	0.228(1)	−0.045(1)	0.126(1)	0.009(2)
C26	0.249(1)	−0.054(1)	0.047(1)	0.009(2)
C27	0.373(1)	−0.063(1)	0.026(1)	0.009(2)
C28	0.474(1)	−0.071(1)	0.085(1)	0.009(2)
C29	0.451(1)	−0.068(1)	0.164(1)	0.009(2)
C30	0.330(1)	−0.050(1)	0.184(1)	0.009(2)
C31	−0.026(1)	−0.104(1)	0.060(1)	0.009(2)
O32	0.059(1)	−0.143(1)	0.075(1)	0.083(5)
O33	−0.110(1)	−0.115(1)	−0.002(1)	0.083(5)
C34	−0.164(1)	−0.171(1)	−0.032(1)	0.009(2)
C35	−0.299(1)	−0.151(1)	−0.065(1)	0.009(2)
C36	−0.172(1)	−0.221(1)	0.030(1)	0.009(2)
C37	−0.073(1)	−0.186(1)	−0.095(1)	0.009(2)
C38	0.105(1)	0.062(1)	0.258(1)	0.009(2)
N39	0.006(1)	0.099(1)	0.283(1)	0.061(4)
C40	−0.105(1)	0.067(1)	0.254(1)	0.009(2)
O41	0.219(1)	0.075(1)	0.278(1)	0.083(5)
C42	−0.227(1)	0.089(1)	0.280(1)	0.009(2)
C43	−0.229(1)	0.112(1)	0.356(1)	0.009(2)
C44	−0.345(1)	0.116(1)	0.390(1)	0.009(2)
C45	−0.460(1)	0.102(1)	0.346(1)	0.009(2)
C46	−0.457(1)	0.077(1)	0.270(1)	0.009(2)
C47	−0.342(1)	0.075(1)	0.235(1)	0.009(2)
C48	0.028(1)	0.160(1)	0.315(1)	0.009(2)
O49	0.001(1)	0.210(1)	0.278(1)	0.083(5)
O50	0.087(1)	0.175(1)	0.386(1)	0.083(5)
C51	0.170(1)	0.226(1)	0.403(1)	0.009(2)
C52	0.080(1)	0.270(1)	0.443(1)	0.009(2)
C53	0.290(1)	0.211(1)	0.459(1)	0.009(2)
C54	0.208(1)	0.251(1)	0.325(1)	0.009(2)
H6	−0.361(7)	−0.338(4)	−0.117(9)	0.05
H7	−0.149(8)	−0.295(4)	−0.148(6)	0.05
H8	0.043(3)	−0.365(3)	−0.143(7)	0.05
H9	0.030(6)	−0.472(3)	−0.088(5)	0.05
H10	−0.181(8)	−0.515(6)	−0.057(4)	0.05
H26	0.168(4)	−0.049(5)	0.001(9)	0.05
H27	0.391(6)	−0.068(4)	−0.036(6)	0.05
H28	0.570(6)	−0.083(6)	0.068(6)	0.05
H29	0.530(4)	−0.074(4)	0.210(6)	0.05
H30	0.312(5)	−0.045(2)	0.246(7)	0.05
H43	−0.140(7)	0.128(3)	0.389(9)	0.05
H44	−0.348(9)	0.136(3)	0.450(5)	0.05
H45	−0.552(9)	0.108(3)	0.371(6)	0.05
H46	−0.547(7)	0.061(4)	0.237(8)	0.05
H47	−0.340(7)	0.058(7)	0.175(6)	0.05

Table 2 Refined atomic coordinates and isotropic displacement parameters of β-DPP-Boc [$P2_1/c$; $a = 6.2280(5)$ Å, $b = 10.2981(2)$ Å, $c = 19.4676(3)$ Å, $\beta = 90.4065(8)°$]. Atom labelling is defined in Fig. 6(a)

Atom	x	y	z	U_{iso}/Å^2
C1	−0.231(1)	0.080(1)	0.031(1)	0.05
N2	−0.272(1)	−0.043(1)	0.062(1)	0.05
C3	−0.115(1)	−0.135(1)	0.048(1)	0.05
C4	−0.030(1)	0.068(1)	−0.006(1)	0.05
C5	−0.112(1)	−0.274(1)	0.066(1)	0.05
C6	0.079(1)	−0.328(1)	0.092(1)	0.05
C7	0.090(1)	−0.459(1)	0.108(1)	0.05
C8	−0.087(1)	−0.534(1)	0.093(1)	0.05
C9	−0.274(1)	−0.481(1)	0.065(1)	0.05
C10	−0.295(1)	−0.348(1)	0.053(1)	0.05
O11	−0.341(1)	0.179(1)	0.041(1)	0.05
C12	−0.386(1)	−0.041(1)	0.124(1)	0.05
O13	−0.363(1)	−0.134(1)	0.163(1)	0.05
O14	−0.573(1)	0.026(1)	0.131(1)	0.05
C15	−0.658(1)	0.074(1)	0.194(1)	0.05
C16	−0.797(1)	0.193(1)	0.176(1)	0.05
C17	−0.467(1)	0.099(1)	0.242(1)	0.05
C18	−0.813(1)	−0.036(1)	0.211(1)	0.05

ment is not necessary, as the pivot point (×) resides on the crystallographic inversion centre. Each Monte Carlo move comprised random displacements of all four variable torsion angles, with global rotation of the structural fragment carried out in every seventh Monte Carlo move. The complete data range $8° \leq 2\theta \leq 60°$ was used in the Monte Carlo calculation.

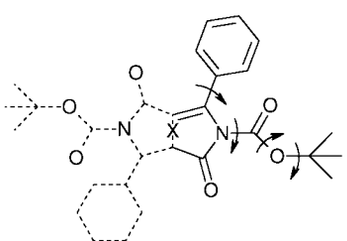

Fig. 4 The structural fragment used in the Monte Carlo structure solution calculation for β-DPP-Boc. The atoms included in the calculation are indicated by the solid line. The pivot point is marked × and the variable torsion angles are defined by arrows.

The parameter S[13] was fixed at $S = 3$ throughout the structure solution calculation, and in total 20 000 Monte Carlo moves were carried out. The best structure solution, corresponding to $R_{wp} = 34.7\%$ (Monte Carlo move number 861), was readily discriminated from "wrong" structures, for which the average value of R_{wp} was about 44%. The trial structure with lowest R_{wp} sampled during the Monte Carlo calculation was used as the starting structural model for Rietveld refinement.

Rietveld refinement was carried out over the complete data range $8° \leq 2\theta \leq 60°$ using the program SR15LS.[37] The overall strategy for Rietveld refinement was the same as that adopted for α-DPP-Boc (see Section 5), except that the background was refined using a background function (rather than a fixed background) and hydrogen atoms were not included. The isotropic displacement parameters were fixed at 0.05 Å^2 for all atoms throughout the refinement. Final convergence was achieved with $R_{wp} = 10.3\%$, $R_p = 7.9\%$ and $\chi^2 = 2.7$ (5200 data points and 64 refined parameters). The experimental and calculated powder diffraction patterns are compared in Fig. 5 and the final refined atomic coordinates are given in Table 2.

The crystal structure of β-DPP-Boc (Fig. 6) contains columns of DPP-Boc molecules stacked along the *a*-axis. The molecules in adjacent columns are packed relative to each other in a parallel arrangement, as shown in Fig. 6(b). The molecular packing arrangements in α-DPP-Boc and β-DPP-Boc differ significantly, as now discussed in detail.

7. Discussion

In both the α and β phases, the DPP-Boc molecules form columns (along the *c*-axis for α-DPP-Boc and the *a*-axis for β-DPP-Boc) as shown in Figs. 3 and 6. One major difference between the structures of the α and β phases concerns the relative packing of these columns of molecules. In α-DPP-Boc, the molecules in adjacent columns are packed relative to each other in a herring-bone arrangement (Fig. 3(b)), whereas in β-DPP-Boc, the molecules in adjacent columns are packed relative to each other in an essentially parallel arrangement (Fig. 6(b)). Although there are some similarities in the packing of molecules along a given column in the α and β phases, the details differ significantly.

The periodic repeat distance along the column axis is approximately three times larger for α-DPP-Boc (17.13 Å) than

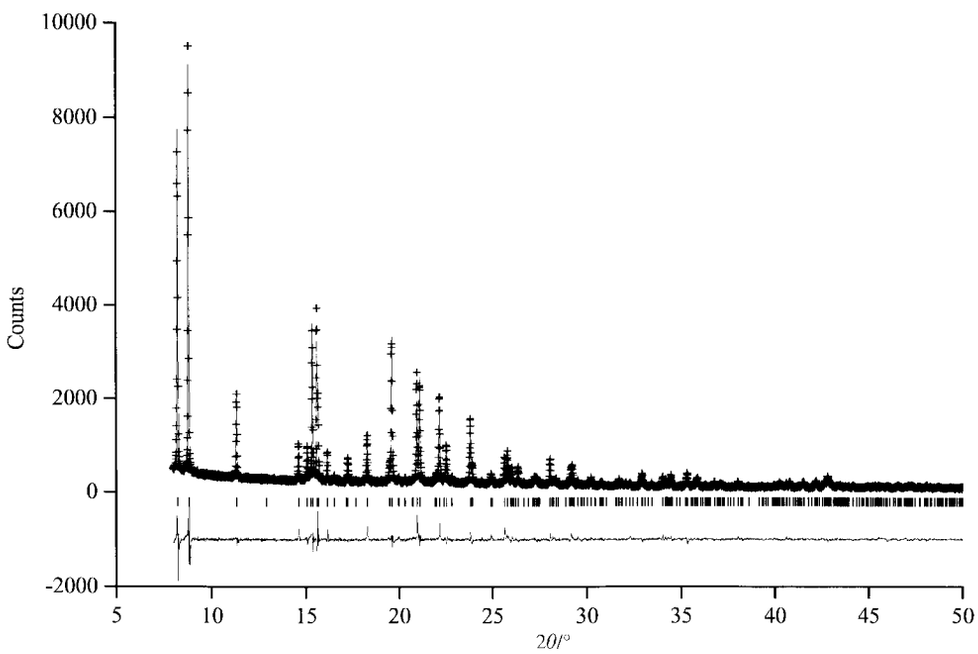

Fig. 5 Experimental (+), calculated (solid line) and difference (bottom) powder diffraction profiles for the final Rietveld refinement of β-DPP-Boc. Reflection positions are marked.

β-DPP-Boc (6.23 Å), reflecting the fact that the asymmetric unit is three times larger for α-DPP-Boc (three half molecules) than β-DPP-Boc (one half molecule). For α-DPP-Boc, there are three molecules in the repeat unit along the column, representing one symmetric molecule (denoted S) flanked by two asymmetric molecules (denoted A). Thus, the molecular packing arrangement along the columns can be envisaged to comprise groups of three molecules stacked as: ···A·S·A···A·S·A···A·S·A···. The intermolecular separation is significantly shorter *within* each group of three molecules (*i.e.* A·S spacing; 5.05 Å) than *between* adjacent groups (*i.e.* A···A spacing; 7.07 Å). These distances between pairs of molecules are measured from the midpoints of the central bonds of the pyrrolo[3,4-*c*]pyrrole units in the two molecules. For β-DPP-Boc, the spacing between each pair of adjacent molecules (related by the lattice translation) is 6.23 Å.

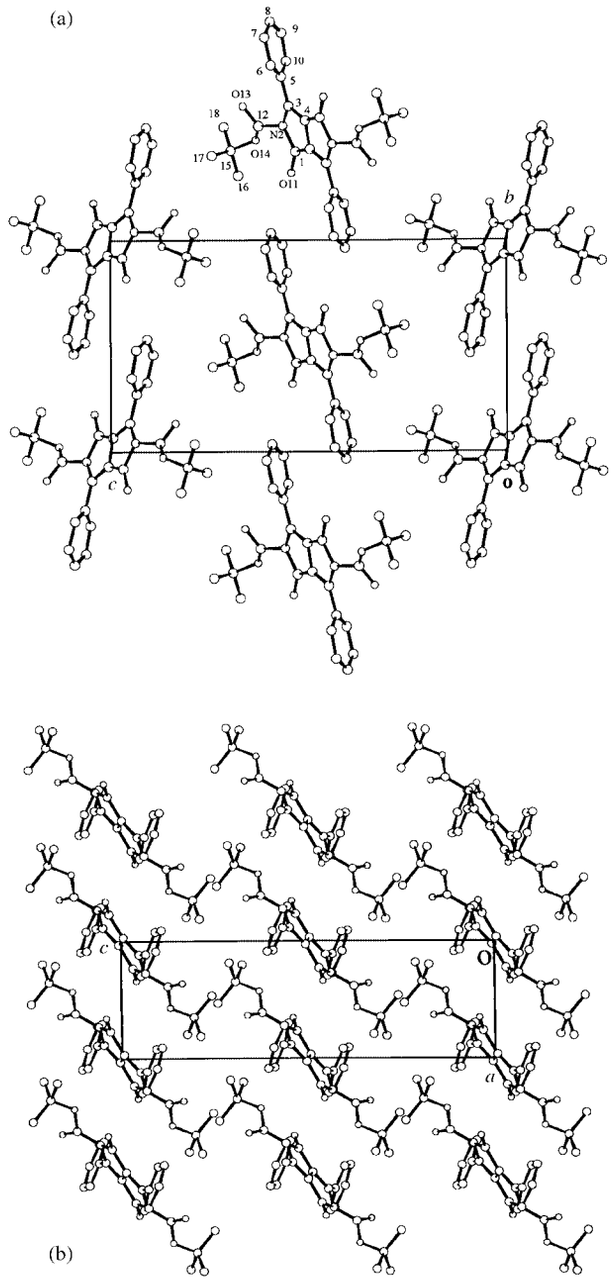

Fig. 6 Crystal structure of β-DPP-Boc viewed (a) along the column axis (*a*-axis) and (b) along the *b*-axis (almost perpendicular to the column axis). The atom labelling scheme (with the label C for each carbon atom omitted for clarity) is defined in (a).

Table 3 Torsion angles defining the angle between the pyrrolo[3,4-*c*]-pyrrole units and the phenyl rings in α-DPP-Boc and β-DPP-Boc, and the corresponding torsion angles in DPP and other DPP derivatives of known structure [*m*-Cl-DPP represents 1,4-dioxo-3,6-bis(3′-chlorophenyl)-1,2,4,5-tetrahydropyrrolo[3,4-*c*]pyrrole; *p*-Cl-DPP represents 1,4-dioxo-3,6-bis(4′-chlorophenyl)-1,2,4,5-tetrahydropyrrolo[3,4-*c*]-pyrrole]

α-DPP-Boc (symmetric molecule)	N2–C3–C5–C6	22.7°
α-DPP-Boc (asymmetric molecule)	N20–C21–C25–C26	35.4°
	N39–C40–C42–C43	−34.9°
β-DPP-Boc	N2–C3–C5–C10	47.2°
DPP[38]		6.9°
m-Cl-DPP[39]		−10.1°
p-Cl-DPP[39]		3.4°

Table 4 Torsion angles defining the conformations of the Boc groups in α-DPP-Boc and β-DPP-Boc

α-DPP-Boc (symmetric molecule)	N2–C12–O14–C15	175.8°
α-DPP-Boc (asymmetric molecule)	N20–C31–O33–C34	−150.5°
	N39–C48–O50–C51	141.9°
β-DPP-Boc	N2–C12–O14–C15	−155.5°

In α-DPP-Boc, the conformations of the Boc groups and the phenyl rings are different for each of the three half molecules in the asymmetric unit. The torsion angles defining the angle between the pyrrolo[3,4-*c*]pyrrole units and phenyl rings in α-DPP-Boc and β-DPP-Boc are listed in Table 3, together with the corresponding torsion angles in DPP and derivatives of DPP of known structure.[38,39] It is clear that the non-planarity is significantly greater for the DPP-Boc molecules (in both the α and β phases) in comparison with the molecules in the other DPP pigments in Table 3. The non-planarity of the phenyl rings with respect to the pyrrolo[3,4-*c*]pyrrole units is particularly substantial for β-DPP-Boc.

The torsion angles defining the conformations of the Boc groups in α-DPP-Boc and β-DPP-Boc are listed in Table 4. Again, there are significant differences in this conformational aspect, particularly between the symmetric and asymmetric molecules in the structure of α-DPP-Boc.

Of the different molecular conformations found in the α and β phases of DPP-Boc, the symmetric molecule in α-DPP-Boc exhibits the greatest degree of planarity, both in terms of the angle between the pyrrolo[3,4-*c*]pyrrole units and the phenyl rings (Table 3) and in terms of the conformation of the Boc groups (Table 4). The relative planarity of this molecule *may* be an important feature facilitating the close intermolecular separation within the groups of three molecules (A·S·A) in the structure of α-DPP-Boc. Within these groups of three molecules (A·S·A), the phenyl rings of the asymmetric molecules are tilted such that they form identifiable edge-to-face interactions with the phenyl rings of the symmetric molecule. The distances between the centre of each phenyl ring of the symmetric molecule and the midpoint of the nearest edge of a phenyl ring of the asymmetric molecule are 3.98 Å and 4.03 Å (note that there is no evidence for such interactions between phenyl rings of adjacent asymmetric molecules in the α phase, nor between adjacent molecules in the β phase). In the α phase, the pyrrolo[3,4-*c*]pyrrole units of the symmetric and asymmetric molecules are essentially parallel to each other, with only a slight displacement in the direction of the planes.

A further contrast between the α and β phases concerns the angle of tilt of the planes of the pyrrolo[3,4-*c*]pyrrole units away from the stacking axis. Thus, the angle between the normal to the plane of the pyrrolo[3,4-*c*]pyrrole units and the stacking axis is about 10° larger for the β phase than the α phase, representing a greater degree of tilting in the β phase—see Figs. 3(b) and 6(b).

As discussed in Section 1, physical and chemical properties may in general differ within a family of polymorphs, as a consequence of structural difference. Indeed, the α and β phases of DPP-Boc differ in colour (different shades of orange/yellow).

However, as discussed in Section 1, the main technological importance of DPP-Boc is not in its own colouristic properties, but rather in terms of its application as a latent pigment for the production of DPP *via* the thermal decomposition reaction. In this regard, we have found that the kinetic aspects of this chemical reaction differ substantially between the α and β phases (for example, the initial rate of reaction is substantially faster for the α phase). Clearly such differences in chemical properties originate from the different structural characteristics of the α and β polymorphs. This issue will be discussed in more detail, together with our studies of kinetic and structural aspects of the chemical transformations in the α and β phases of DPP-Boc, in a forthcoming publication.[10]

Acknowledgements

We are grateful to Ciba Speciality Chemicals (studentship to E. J. M. and postdoctoral fellowship to B. M. K.), University College London (studentship to E. J. M.), and EPSRC (postdoctoral fellowship to M. T. and award of beam-time at Daresbury Laboratory) for supporting the research described in this paper. The University of London Intercollegiate Research Service (Dr A. E. Aliev and Dr P. J. Barrie) is thanked for providing facilities for solid state NMR spectroscopy. Professor W. I. F. David is thanked for providing the SR15LS program for Rietveld refinement.

References

1 J. D. Dunitz, *Pure Appl. Chem.*, 1991, **63**, 177.
2 M. R. Caira, *Top. Curr. Chem.*, 1998, **198**, 164.
3 J. Bernstein, R. J. Davey and J.-O. Henck, *Angew. Chem.*, *Int. Ed. Engl.*, 1999, **38**, 3441.
4 G. D. Potts, W. Jones, J. F. Bullock, S. J. Andrews and S. J. Maginn, *J. Chem. Soc.*, *Chem. Commun.*, 1994, 2565.
5 J. Mizuguchi, A. C. Rochat and G. Rhis, *Acta Crystallogr.*, *Sect. C*, 1990, **46**, 1899.
6 J. Mizuguchi, M. Arita and G. Rhis, *Acta Crystallogr.*, *Sect. C*, 1991, **47**, 1952.
7 B. J. Mann, E. N. Duesler, I. C. Paul and D. Y. Curtin, *J. Chem. Soc.*, *Perkin Trans. 2*, 1981, 1577.
8 J. S. Zambounis, Z. Hao and A. Iqbal, *Nature*, 1997, **388**, 131.
9 J. S. Zambounis, Z. Hao and A. Iqbal, US Patent No. 5,484,943, 1996.
10 E. J. MacLean, K. D. M. Harris, A. F. M. Iqbal and Z. Hao, manuscript in preparation.
11 Ciba Specialty Chemicals, unpublished results.
12 E. J. MacLean, PhD Thesis, University of London, 1997.
13 K. D. M. Harris, M. Tremayne, P. Lightfoot and P. G. Bruce, *J. Am. Chem. Soc.*, 1994, **116**, 3543.
14 M. Tremayne, B. M. Kariuki and K. D. M. Harris, *Angew. Chem.*, *Int. Ed. Engl.*, 1997, **36**, 770.
15 K. D. M. Harris, B. M. Kariuki and M. Tremayne, *Mater. Sci. Forum*, 1998, **278**–**291**, 32.
16 H. M. Rietveld, *J. Appl. Crystallogr.*, 1969, **2**, 65.
17 K. D. M. Harris and M. Tremayne, *Chem. Mater.*, 1996, **8**, 2554.
18 D. M. Poojary and A. Clearfield, *Acc. Chem. Res.*, 1997, **30**, 414.
19 N. Masciocchi and A. Sironi, *J. Chem. Soc.*, *Dalton Trans.*, 1997, 4643.
20 A. Meden, *Croat. Chim. Acta*, 1998, **71**, 615.
21 D. Louër, *Acta Crystallogr.*, *Sect. A*, 1998, **54**, 992.
22 J. M. Newsam, M. W. Deem and C. M. Freeman, in *Accuracy in Powder Diffraction II*; *NIST Special Publ. No. 846*, 1992, p. 80.
23 D. Ramprasad, G. P. Pez, B. H. Toby, T. J. Markley and R. M. Pearlstein, *J. Am. Chem. Soc.*, 1995, **117**, 10694.
24 Y. G. Andreev, P. Lightfoot and P. G. Bruce, *Chem. Commun.*, 1996, 2169.
25 Y. G. Andreev, G. S. MacGlashan and P. G. Bruce, *Phys. Rev. B*, 1997, **55**, 12011.
26 W. I. F. David, K. Shankland and N. Shankland, *Chem. Commun.*, 1998, 931.
27 G. E. Engel, S. Wilke, O. König, K. D. M. Harris and F. J. J. Leusen, *J. Appl. Crystallogr.*, 1999, **32**, 1169.
28 B. M. Kariuki, H. Serrano-González, R. L. Johnston and K. D. M. Harris, *Chem. Phys. Lett.*, 1997, **280**, 189.
29 K. D. M. Harris, R. L. Johnston and B. M. Kariuki, *Acta Crystallogr.*, *Sect. A*, 1998, **54**, 632.
30 P. Calcagno, B. M. Kariuki, K. D. M. Harris, D. Philp and R. L. Johnston, *Angew. Chem.*, *Int. Ed. Engl.*, 1999, **38**, 831.
31 K. Shankland, W. I. F. David and T. Csoka, *Z. Kristallogr.*, 1997, **212**, 550.
32 K. Shankland, W. I. F. David, T. Csoka and L. McBride, *Int. J. Pharm.*, 1998, **165**, 117.
33 S. P. Collins, R. J. Cernik, P. Pattison, A. M. T. Bell and A. N. Fitch, *Rev. Sci. Instrum.*, 1992, **63**, 1013.
34 E. J. MacLean, H. F. F. Millington and C. C. Tang, *Mater. Sci. Forum*, 2000, **321**–**324**, 212.
35 J. W. Visser, *J. Appl. Crystallogr.*, 1969, **2**, 89.
36 A. C. Larson and R. B. Von Dreele, *Los Alamos Laboratory Report No.* LA-UR-86-748, Los Alamos Laboratory, NM, USA.
37 W. I. F. David, R. M. Ibberson and J. C. Matthewman, *Rutherford Appleton Lab. Report* RAL-92-032, 1992.
38 J. Mizuguchi, A. Grubenmann, G. Wooden and G. Rhis, *Acta Crystallogr.*, *Sect. B*, 1992, **48**, 696.
39 J. Mizuguchi, A. Grubenmann and G. Rhis, *Acta Crystallogr.*, *Sect. B*, 1993, **49**, 1056.